Physics Letters A 373 (2009) 3594–3600

Contents lists available at ScienceDirect

Physics Letters A

www.elsevier.com/locate/pla

Wave properties of an annular periodic multilayer structure containing the single-negative materials

Mei-Soong Chen [a,*], Chien-Jang Wu [b], Tzong-Jer Yang [c]

[a] Department of Electrophysics, National Chiao-Tung University, Hsinchu 300, Taiwan
[b] Institute of Electro-Optical Science and Technology, National Taiwan Normal University, Taipei 116, Taiwan
[c] Department of Electrical Engineering, Chung Hua University, Hsinchu 300, Taiwan

ARTICLE INFO

Article history:
Received 11 June 2009
Received in revised form 23 July 2009
Accepted 27 July 2009
Available online 4 August 2009
Communicated by R. Wu

PACS:
41.20.Jb
42.70.Qs
74.25.Gz

Keywords:
Annular Bragg reflectors
Single-negative materials
Transfer matrix method
Optical properties

ABSTRACT

The optical properties of an annular periodic multilayer structure containing two kinds of single-negative materials are theoretically investigated based on the transfer matrix method of the cylindrical waves. At the azimuthal mode number $m \geqslant 1$ and near the magnetic plasma frequency and the electronic plasma frequency for the TE wave and TM wave, respectively, we find that there is an additional high-reflectance band and some reflection dips exist when the plasma frequency is located in the photonic band gap. These two special features arising from the higher order azimuthal mode of the cylindrical waves are not seen in the planar one-dimensional Bragg reflector consisting of the single-negative materials. Such filtering responses provide a feasible way of designing a narrowband resonator without physically introducing any defect layer in the structure.

1. Introduction

The electromagnetic metamaterials with both the negative permittivity ($\varepsilon < 0$) and negative permeability ($\mu < 0$) first predicted by Veselago early in 1968 [1] are called the double-negative (DNG) materials. A significant result coming from the DNG material is that its index of refraction is negative. Thus, a DNG material is commonly referred to as the negative-index material (NIM). The existence of this kind material was respectively experimentally demonstrated by Smith et al. [2,3] and one of the distinctive applications of the DNG materials was presented by Pendry et al. [4].

In addition to the DNG materials [5–7], the single-negative (SNG) materials also attract much attention recently. An SNG material means that only one of the two material parameters, ε and μ, is negative [8–10]. Thus an SNG material could be the epsilon-negative (ENG) medium with $\varepsilon < 0$ and $\mu > 0$ or the mu-negative (MNG) medium with $\mu < 0$ and $\varepsilon > 0$. It is known that a photonic band gap (PBG) could be formed as a consequence of the interference of Bragg scattering in a periodical layer structure like a one-dimensional photonic crystals (1DPCs) and Bragg reflectors (1DBRs). In a usual 1DBR made of all positive-index materials, the PBG is called the Bragg gap, which is proven to be strongly dependent on the lattice constant and the disorder of a device as well. However, for the SNG materials ε and μ are frequency-dependent, so that we have $\varepsilon < 0$ and $\mu > 0$ or $\mu < 0$ and $\varepsilon > 0$ within a certain frequency range, which is called the SNG frequency range. Therefore, the PBG in the SNG frequency range is called the SNG gap. For a 1DBR consisting of ENG–MNG bilayers, it is known that the SNG gap is fundamentally different from the Bragg gap. There have been many reports on the 1D plane BRs (1DPBRs) containing SNG materials [11–14].

Besides the simple 1DPBRs or 1DPC, two-dimensional BRs (2DBRs) are also important in the photonic and physical communities. A similar version 2DBR is a periodic bilayer structure in an annular geometry called an annular Bragg reflector (ABR). An ABR plays an important and useful role in modern laser system with a feature of vertical emission [15]. Similar device like the annular Bragg resonator is also available in the present [16].

In this Letter, based on the transfer matrix method for the cylindrical Bragg waves developed by Kaliteevski et al. [17], we shall theoretically investigate the optical properties in an ABR consisting of the MNG–ENG materials. With the fact that the field solutions of the cylindrical Bragg waves for both TE and TM waves are dependent on the azimuthal mode number denoted by m,

* Corresponding author. Tel.: +886 3 5720635; fax: +886 3 5725230.
E-mail address: cathy.ep91g@nctu.edu.tw (M.-S. Chen).

0375-9601/$ – see front matter
doi:10.1016/j.physleta.2009.07.075

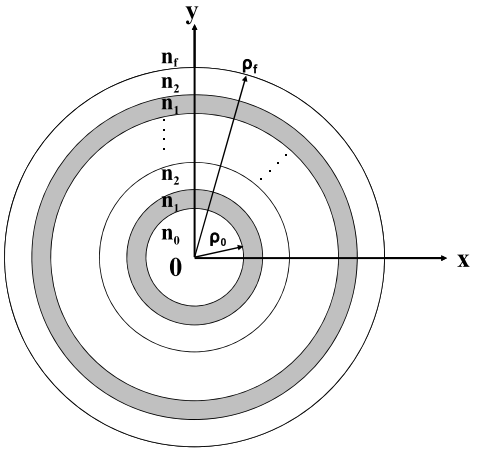

Fig. 1. The top view of the ABR, where MNG and ENG layers are taken to be with indices n_1 and n_2, respectively. The thicknesses of MNG and ENG layers are d_1 and d_2, and ρ_0 is the starting radius.

optical reflectance will be studied at different m-number. The frequency-dependent reflectance at $m = 0$ is first shown to be nearly identical to that of 1DPBR containing the SNG materials. Next, the reflectance spectra are plotted and compared at different values of m. At $m \geqslant 1$, it is found that there exist some novelties compared with the usual PBR. Furthermore, we insert a defect layer in the periodic multilayers and conclude the property of the SNG gap for an ABR is insensitive to the disorder as same as the one-dimensional BR.

2. Theory

We first introduce an ABR consisting of the MNG/ENG double layers. The relative permittivity and permeability for a MNG material are given by [11,12]

$$\varepsilon_m = a, \qquad \mu_m = 1 - \frac{\omega_{mp}^2}{\omega^2}, \tag{1}$$

whereas those of an ENG material are

$$\varepsilon_e = 1 - \frac{\omega_{ep}^2}{\omega^2}, \qquad \mu_e = b, \tag{2}$$

where a and b are positive constants, and ω_{mp} and ω_{ep} are the magnetic plasma frequency and the electronic plasma frequency respectively. It is seen from Eqs. (1) and (2) that the SNG frequency range exist when the frequency satisfies $\omega < \min\{\omega_{mp}, \omega_{ep}\}$ whereas the materials will be double-positive (DPS) if $\omega > \max\{\omega_{mp}, \omega_{ep}\}$.

The top view of the ABR is depicted in Fig. 1, where ρ_0 is called the starting radius, n_1-layer is the MNG material, and n_2-layer is the ENG material. The cylindrical wave is assumed to be radiated from the axis of symmetry, $\rho = 0$, and to be incident normally on the first interface at $\rho = \rho_0$. The reflectance at $\rho = \rho_0$ can be analytically analyzed by making use of the transfer matrix method in cylindrical Bragg wave [17]. There are two possible polarizations for the cylindrical Bragg wave, i.e., E-polarization (TE) and the H-polarization (TM). Let us first formulate the problem for the TE wave. Assuming the temporal part proportional to $e^{j\omega t}$ for all fields, the nonzero fields for the TE wave are E_z, H_ϕ, and H_ρ, where E_z satisfies the following governing equation,

$$\rho \frac{\partial}{\partial \rho}\left(\rho \frac{\partial E_z}{\partial \rho}\right) - \rho^2 \frac{1}{\mu}\frac{\partial \mu}{\partial \rho}\frac{\partial E_z}{\partial \rho} + \frac{\partial}{\partial \phi}\left(\frac{\partial E_z}{\partial \phi}\right) + \omega^2 \mu \varepsilon \rho^2 E_z = 0. \tag{3}$$

The solution for E_z can be expressed as $E_z = V(\rho)\Phi(\phi) = V(\rho)e^{jm\phi}$, where V is

$$V(\rho) = A J_m(k\rho) + B Y_m(k\rho), \tag{4}$$

where A and B are the constants, J_m is a Bessel function, Y_m is a Neumann function and $k = \omega\sqrt{\mu\varepsilon}$ is the wave number of the medium. The index m is an integer and is referred to as the azimuthal mode number. Similarly, the tangential magnetic field can be expressed as $H_\phi = U(\rho)e^{jm\phi}$, where $U(\rho)$ is given by

$$U(\rho) = -jp\big(A J'_m(k\rho) + B Y'_m(k\rho)\big), \tag{5}$$

where $p = \sqrt{\varepsilon/\mu}$ is the intrinsic admittance of the medium.

Eqs. (4) and (5) enable us to establish the matrix relationship for the first layer with matrix $\mathbf{M}_1$ (with refractive index n_1 and interfaces at $\rho = \rho_0$ and ρ_1) [17]. Likewise, for ith layer the matrix $\mathbf{M}_i$ can be obtained by the replacements, $\rho_0 \to \rho_{i-1}$, and $\rho_1 \to \rho_i$. For a periodic bilayer structure as in Fig. 1 we have $\varepsilon_i = \varepsilon_1$ if $i =$ odd, and $\varepsilon_i = \varepsilon_2$ if $i =$ even. Thus, the matrix equation for the total system matrix $\mathbf{M}$ is given by

$$\begin{bmatrix} V(\rho_f) \\ U(\rho_f) \end{bmatrix} = \mathbf{M}_{2N}\cdots\mathbf{M}_2\mathbf{M}_1 \left[\begin{pmatrix} V(\rho_0) \\ U(\rho_0) \end{pmatrix}\right] = \mathbf{M}\begin{bmatrix} V(\rho_0) \\ U(\rho_0) \end{bmatrix}. \tag{6}$$

Based on the matrix elements in Eq. (6), the matrix elements of the inverse of $\mathbf{M}$ denoted by M'_{11}, M'_{12}, M'_{21} and M'_{22} can be readily obtained and then the reflection and transmission coefficients are determined by the following equations [17],

$$r_d = \frac{(M'_{21} + jp_0 C^{(2)}_{m0} M'_{11}) - jp_f C^{(2)}_{mf}(M'_{22} + jp_0 C^{(2)}_{m0} M'_{12})}{(-jp_0 C^{(1)}_{m0} M'_{11} - M'_{21}) - jp_f C^{(2)}_{mf}(-jp_0 C^{(1)}_{m0} M'_{12} - M'_{22})}, \tag{7}$$

$$t_d = 4\sqrt{\varepsilon_0/\mu_0} \times \big(\pi K \rho_0 H^{(2)}_m(k_0\rho_0) H^{(1)}_m(k_0\rho_0)\big[\big(-jp_0 C^{(1)}_{m0} M'_{11} - M'_{21}\big) - jp_f C^{(2)}_{mf}\big(-jp_0 C^{(1)}_{m0} M'_{12} - M'_{22}\big)\big]\big)^{-1}, \tag{8}$$

where $p_0 = \sqrt{\varepsilon_0/\mu_0}$ and $p_f = \sqrt{\varepsilon_f/\mu_f}$ are the admittances of the starting and the last medium for the incident wave, $K = \omega\sqrt{\mu_0\varepsilon_0}$ is the free-space wave number, and

$$C^{(1,2)}_{ml} = \frac{H^{(1,2)\prime}_m(k_l\rho_l)}{H^{(1,2)}_m(k_l\rho_l)}, \quad l = 0, f, \tag{9}$$

where $H^{(1)}_m$ and $H^{(2)}_m$ are the Hankel function of the first and second kind. Eqs. (7) and (8) then leads to the reflectance R and the transmittance T, i.e.,

$$R = |r_d|^2, \qquad T = \frac{n_f}{n_0}|t_d|^2, \tag{10}$$

where n_0 and n_f are respectively the refractive indices of the starting and the final media. By simply replacing $\varepsilon \leftrightarrow \mu$, and $j \leftrightarrow -j$ in the above formulations, the corresponding results for the TM wave can be readily obtained.

In the above formulations, we have considered that the input signal is an outgoing cylindrical wave that is uniformly radiated at $\rho = 0$ and impinges normally on $\rho = \rho_0$. Our goal is to calculate the reflectance at one point on $\rho = \rho_0$. However, there should be a reflected wave at the opposite end to this point and it can be regarded as the secondary input signal for the considered point. This secondary signal has been assumed to be neglected for the convenience of formulation. Technically, this secondary source can be eliminated by placing a receiving antenna or a metallic absorber at $\rho = 0$. And the above formulations are thus acceptable and reasonable.

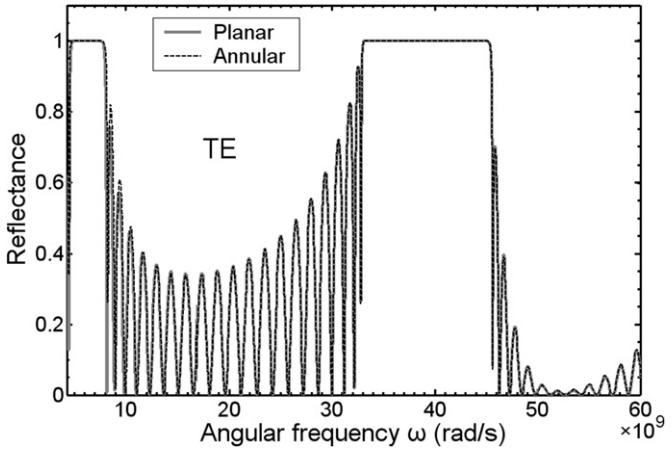

Fig. 2. Calculated reflectance spectra for MNG/ENG Bragg reflectors, where the gray solid is for the PBR, and the dashed line is for the ABR.

3. Numerical results and discussion

In what follows we will present the numerical results for the optical reflectance. We suppose that the ABR is immersed in free space, i.e., $n_0 = n_f = 1$. The SNG material parameters are $a = 3.5$, $b = 1.2$, $\omega_{mp} = 10^{10}$ rad/s, and $\omega_{ep} = 1.3 \times 10^{10}$ rad/s [12]. This indicates that the SNG frequency range exist under the condition of $\omega < 10^{10}$ rad/s. The thicknesses of the MNG and ENG layers are $d_1 = 10$ mm and $d_2 = 5$ mm, and the number of the periods is $N = 21$.

We first investigate the geometric effect on the reflection response for both the ABR and PBR. In Fig. 2, we plot the frequency-dependent TE-reflectance, where the dashed curve is for ABR with $\rho_0 = 28$ mm at the lowest azimuthal mode, $m = 0$, and the gray solid curve is for PBR. It is seen that both of the reflection spectra almost coincide, indicating that at $m = 0$ the geometric difference due to the curved interfaces in ABR nearly has no effect on the reflectance compared to the PBR. In addition, there are two high-reflection band gaps. The narrow one at frequency lower than 10^{10} rad/s is referred to as the SNG gap. The wide band gap at frequency higher than 3×10^{10} rad/s with DPS materials is the usual Bragg gap (BG). The fundamental features between SNG gap and BG are well described in Refs. [11–14].

Because the optical properties at $m = 0$ for an ABR is nearly the same as the usual PBR, we thus study the effects due to field solutions at the higher modes. The TE-reflectance for $m = 0$ (a), 1 (b), 2 (c), and 3 (d) are plotted in Figs. 3, where $\rho_0 = 30$ mm is used. It is of interest to find that at $m \geqslant 1$ an additional PBG appear near $\omega_{mp} = 10^{10}$ rad/s. Such a PBG is referred to as the near-zero-n gap for the MNG material, because within this gap the refractive index of the MNG material is much less one and very close to zero, and this additional PBG is referred to as the MNG gap or the magnetic gap. The MNG gap is enhanced as m increases. At $m = 2$, this additional gap wider than $m = 1$, is not pure SNG gap but a mixed gap of SNG and MNG gap. At $m = 3$, a wider flat top mixed gap is obtained, as shown in Fig. 3(d). In Fig. 4, we plot the TM-reflectance for $m = 0$ (a), 1 (b), 2 (c), and 3 (d) at $\rho_0 = 30$ mm. Similar results in Fig. 3 can also be obtained for the TM wave. Here an additional gap is now near $\omega_{ep} = 1.3 \times 10^{10}$ rad/s, and the additional PBG can be called the ENG gap or the electric gap. This ENG gap will interact with SNG gap considerably at $m > 1$ and then again merges as wider PBG in Fig. 4(d). The results illustrate the effects of the higher-mode cylindrical Bragg wave. In addition, the values in the plasma frequencies, ω_{mp} and ω_{ep}, will determine the position of the additional MNG or ENG gap. It is evident that MNG gap is due to the existence of radial component of the magnetic field H_ρ of

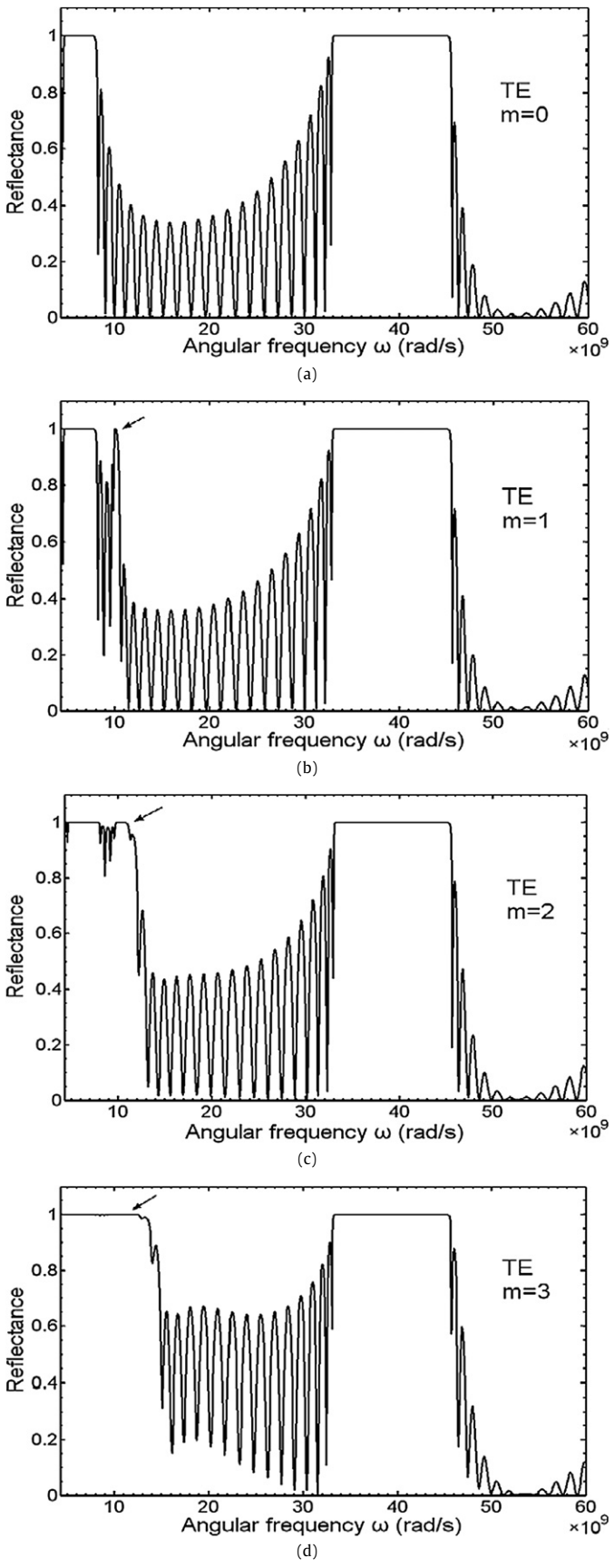

Fig. 3. Calculated reflectance spectra of TE wave for the ABR at different azimuthal modes (a) $m = 0$, (b) $m = 1$, (c) $m = 2$ and (d) $m = 3$, respectively, under the conditions of $a = 3.5$, $b = 1.2$, $\omega_{mp} = 10^{10}$ rad/s, $\omega_{ep} = 1.3 \times 10^{10}$ rad/s, $d_1 = 10$ mm, $d_2 = 5$ mm, $\rho_0 = 30$ mm and $N = 21$.

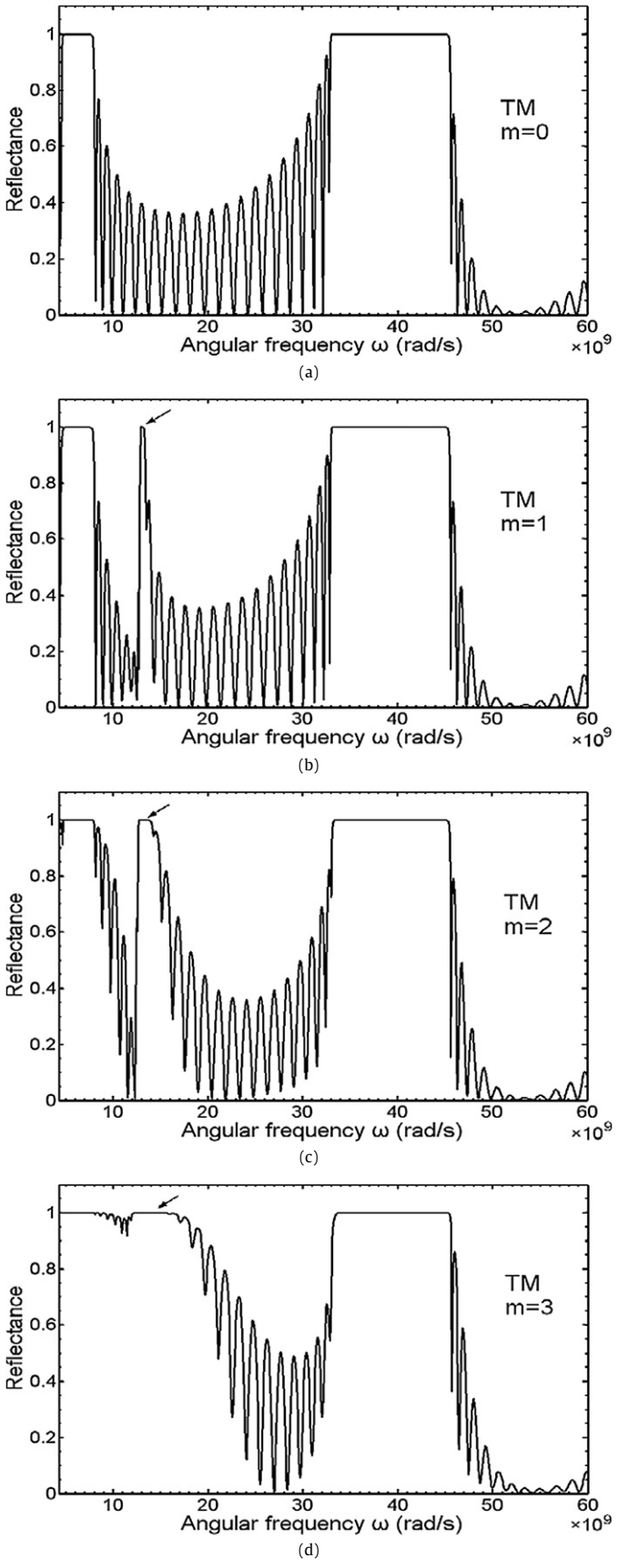

Fig. 4. Calculated reflectance spectra of TM wave for the ABR at different azimuthal mode (a) $m = 0$, (b) $m = 1$, (c) $m = 2$ and (d) $m = 3$, respectively, under the conditions of $a = 3.5$, $b = 1.2$, $\omega_{mp} = 10^{10}$ rad/s, $\omega_{ep} = 1.3 \times 10^{10}$ rad/s, $d_1 = 10$ mm, $d_2 = 5$ mm, $\rho_0 = 30$ mm and $N = 21$.

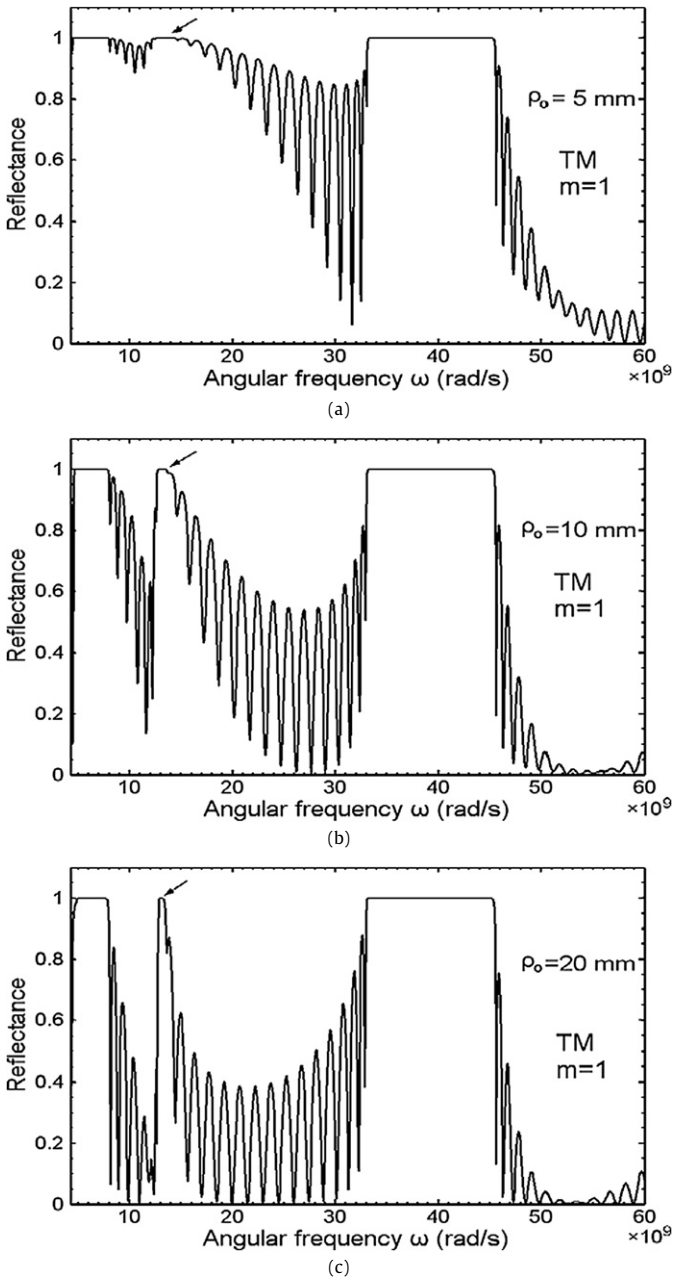

Fig. 5. Calculated reflectance spectra of TM wave at azimuthal mode $m = 1$ for the ABR at different starting radii $\rho_0 = 5$ mm (a), $\rho_0 = 10$ mm (b) and $\rho_0 = 20$ mm (c), respectively, under the conditions of $a = 3.5$, $b = 1.2$, $\omega_{mp} = 10^{10}$ rad/s, $\omega_{ep} = 1.3 \times 10^{10}$ rad/s, $d_1 = 10$ mm, $d_2 = 5$ mm and $N = 21$.

TE wave, and ENG gap is caused by E_ρ of TM wave. Moreover, the higher-order mode causes a strong interaction between the MNG (or ENG) gap and SNG gap, leading to a wider mixed gap. These special results arising from the higher order azimuthal mode of the cylindrical waves are not found in the usual PBR containing of SNG materials. The additional MNG and ENG gap suggest that the ABR could be used to design a narrowband transmission filter or an annular resonator without introducing any physical defect layer in the structure.

In Figs. 5 and 6, we plot TM-reflectance spectra of the ABR for three different starting radii at $m = 1$ and $m = 2$, respectively. (The reflectance spectra of TM wave for $\rho_0 = 30$ mm at both $m = 1$ and $m = 2$ are shown in Fig. 4.) It is seen that the side lobes near the upper bandedge of SNG gap are highly enhanced as the starting radius decreases. Thus, the gap near 10^{10} rad/s is effectively en-

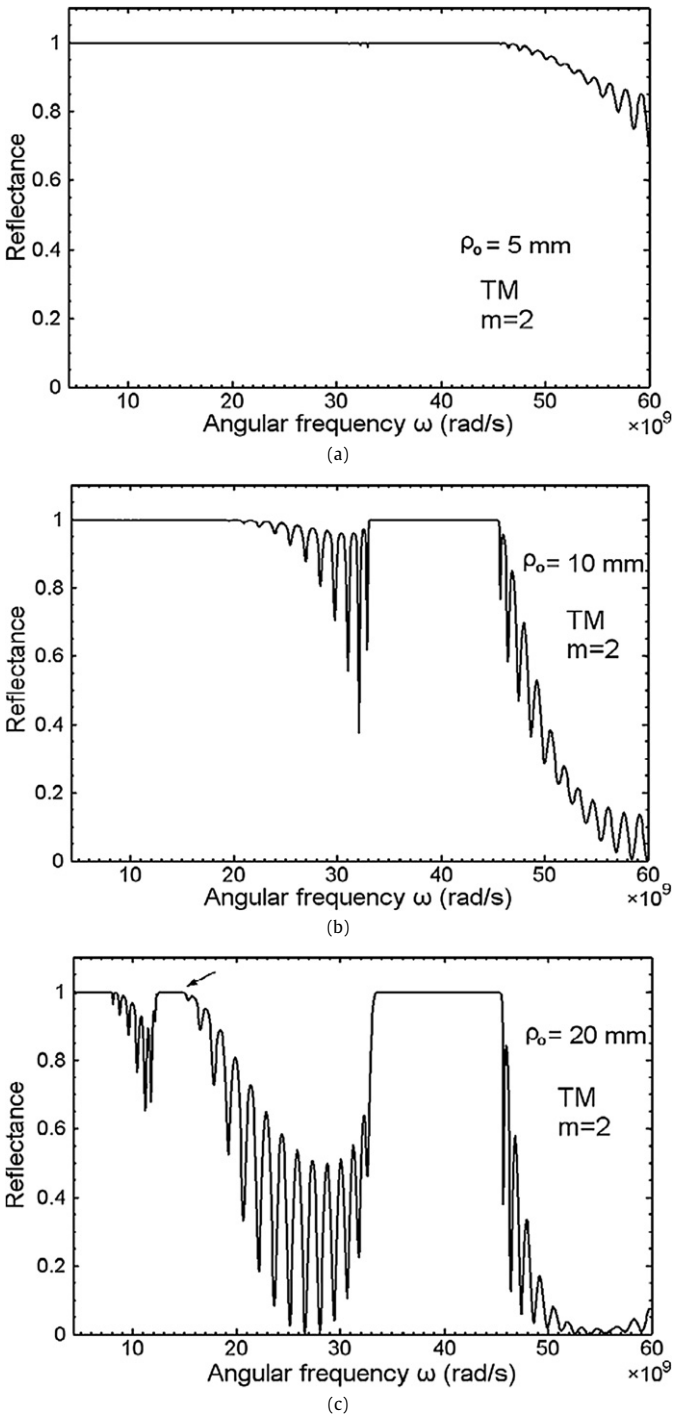

Fig. 6. Calculated reflectance spectra of TM wave at azimuthal mode $m = 2$ for the ABR at different starting radii $\rho_0 = 5$ mm (a), $\rho_0 = 10$ mm (b) and $\rho_0 = 20$ mm (c), respectively, under the conditions of $a = 3.5$, $b = 1.2$, $\omega_{mp} = 10^{10}$ rad/s, $\omega_{ep} = 1.3 \times 10^{10}$ rad/s, $d_1 = 10$ mm, $d_2 = 5$ mm and $N = 21$.

larged at $\rho_0 = 5$ mm. The results suggest that care therefore should be taken in the choice of the starting radius for designing an ABR.

Next, we shall investigate the PBG which the magnetic plasma frequency ω_{mp} and the electronic plasma frequency ω_{ep} are located within. To reach this end, the SNG material parameters are chosen as $a = 6$, $b = 2.5$, $\omega_{mp} = 4 \times 10^{10}$ rad/s, and $\omega_{ep} = 4.5 \times 10^{10}$ rad/s [7,9,13] and the thicknesses of MNG and ENG layers are also changed to be $d_1 = 6$ mm, $d_2 = 3$ mm. The starting radius, $\rho_0 = 22$ mm and number of periods $N = 6$, are taken in our calculation. In Fig. 7 and Fig. 8, we see that ω_{mp} and ω_{ep} are

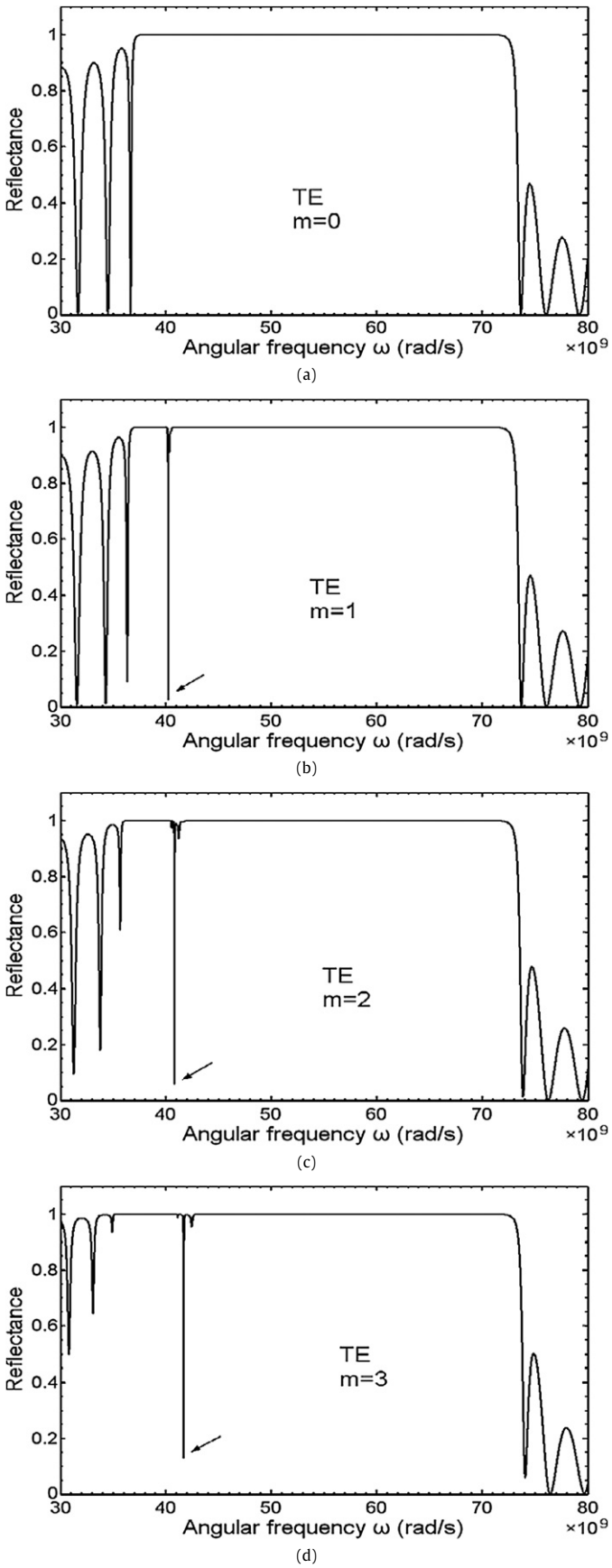

Fig. 7. Calculated reflectance spectra of TE wave for the ABR at different azimuthal mode $m = 0$ (a), $m = 1$ (b), $m = 2$ (c), and $m = 3$ (d), respectively, under the conditions of $a = 6$, $b = 2.5$, $\omega_{mp} = 4 \times 10^{10}$ rad/s, $\omega_{ep} = 4.5 \times 10^{10}$ rad/s, $d_1 = 6$ mm, $d_2 = 3$ mm, $\rho_0 = 22$ mm and $N = 6$.

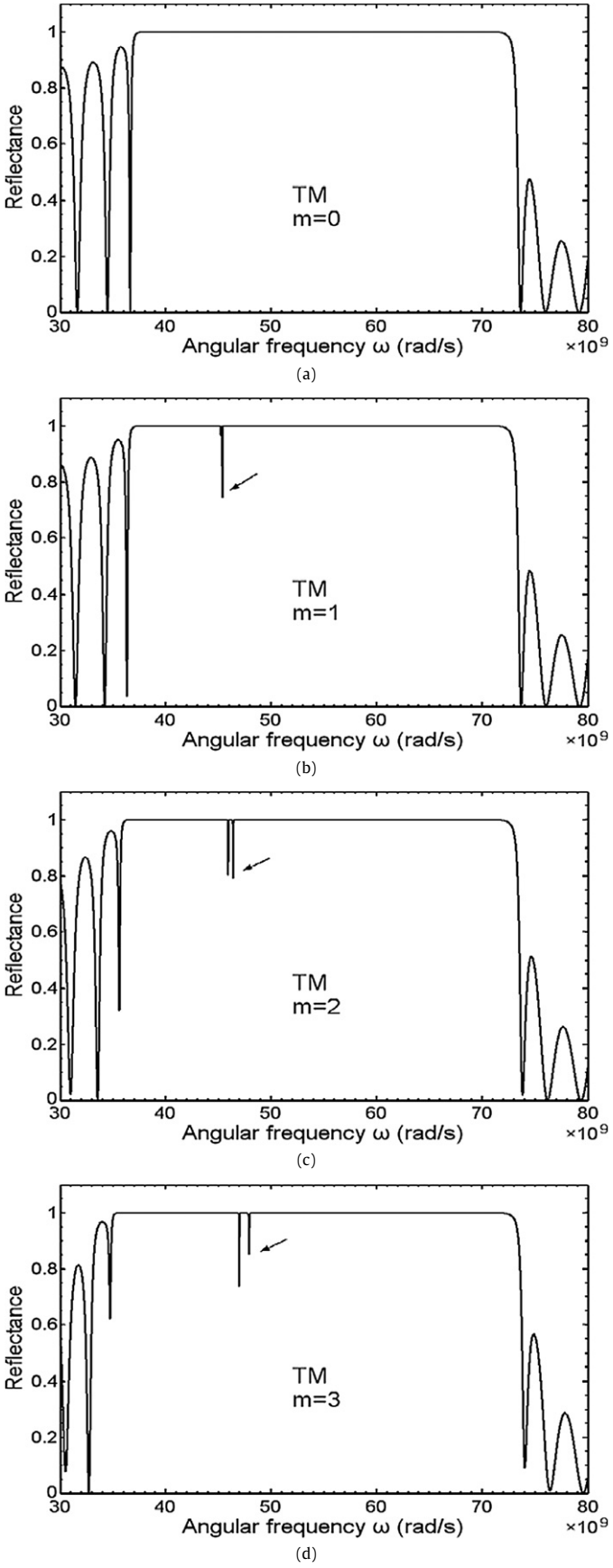

Fig. 8. Calculated reflectance spectra of TM wave for the ABR at different azimuthal mode $m = 0$ (a), $m = 1$ (b), $m = 2$ (c) and $m = 3$ (d), respectively, under the conditions of $a = 6$, $b = 2.5$, $\omega_{mp} = 4 \times 10^{10}$ rad/s, $\omega_{ep} = 4.5 \times 10^{10}$ rad/s, $d_1 = 6$ mm, $d_2 = 3$ mm, $\rho_0 = 22$ mm and $N = 6$.

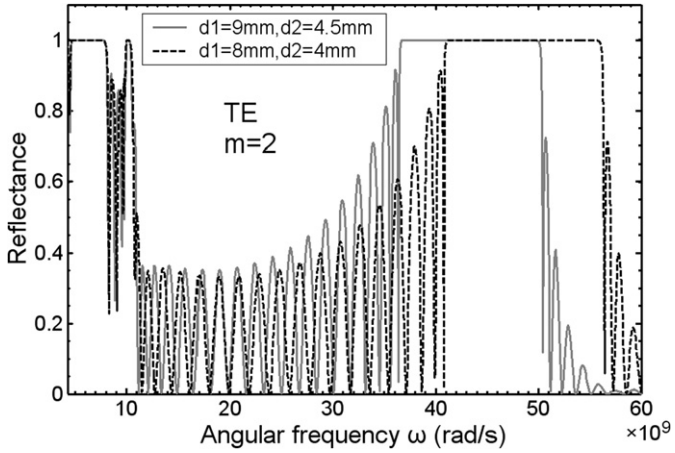

Fig. 9. Calculated reflectance spectra of TE wave at azimuthal mode $m = 2$ for the ABR, under the conditions of $a = 3.5$, $b = 1.2$, $\omega_{mp} = 10^{10}$ rad/s, $\omega_{ep} = 1.3 \times 10^{10}$ rad/s, $\rho_0 = 60$ mm and $N = 21$. The gray solid is for $d_1 = 9$ mm, $d_2 = 4.5$ mm. The dashed line is for $d_1 = 8$ mm, $d_2 = 4$ mm (scaled by 8/9).

located within the PBG. Some features are to be noted. There are dips near ω_{mp} within the PBG at mode $m \geqslant 1$ for TE wave, whereas dips appearing near ω_{ep} in the PBG for TM wave. The dip in TM wave is shallower compared with the TE wave. The appearance of such dips in reflectance is mainly due to the higher azimuthal mode of the cylindrical wave, which, in fact, does not show up in the PBR in the normal-incidence case. In addition, these dips in the PBG are related to the field component H_ρ of TE wave and E_ρ of TM wave, respectively. The deep dip in TE wave enables us to design a circular transmission narrowband filter or resonator without introducing any physical defect. Moreover, a multi-resonance filter is also possible because of the presence of the multiple dips in the reflection response.

It should be noted that the SNG material parameters and the film thicknesses in plotting Figs. 7 and 8 are different from in Figs. 2–6. We use these because the SNG gap is insensitive to the lattice constant and the SNG gap midfrequency is invariant of the ratio of the thickness (see Ref. [12]), it is thus difficult to change the position of the SNG gap in the spectra. In Figs. 2–6, the magnetic plasma frequency ω_{mp} and the electronic plasma frequency ω_{ep} are very close to the SNG gap. If we only change the film thicknesses but use the same values of the plasma frequencies as in Figs. 2–6 to achieve the condition that the plasma frequencies are located within the PBG, this PBG will approach to the SNG gap, which may lead to a confusion in the dips as well as the band edges. Moreover, the PBG may even overlap the SNG gap, which also makes the condition more complicated.

The thickness-dependent band structure in plotted in Fig. 9, where we take a fixed thickness ratio of the two constituent layers with different lattice constants. It is seen that SNG gap is nearly invariant for a fixed thickness ratio, robust to the variation in the lattice constant. However, the Bragg gap is strongly affected by the variation in the lattice constant. That is, the change in the lattice constant leads to a shift in the Bragg gap. In addition, the gap is enhanced as the lattice constant is decreased. These features in SNG and Bragg gaps are also seen in the usual SNG PBR. Conclusively, the fundamental optical properties are proven to be preserved even in the ABR where the boundaries are geometrically changed from the planar shape to the annular one.

Finally, let us consider ABR containing a defect layer D with $\varepsilon_d = 1.8$, $\mu_d = 1.8$ and $d_d = 45$ mm. The structure is denoted as $(\mathrm{MNG/ENG})^6\mathrm{D}(\mathrm{MNG/ENG})^6$. Here we take the material parameters of MNG and ENG as $a = 1.5$, $b = 1.5$, $\omega_{mp} = 10^{10}$ rad/s, and $\omega_{ep} = 10^{10}$ rad/s. For convenience of comparison, the reflectance of ABR

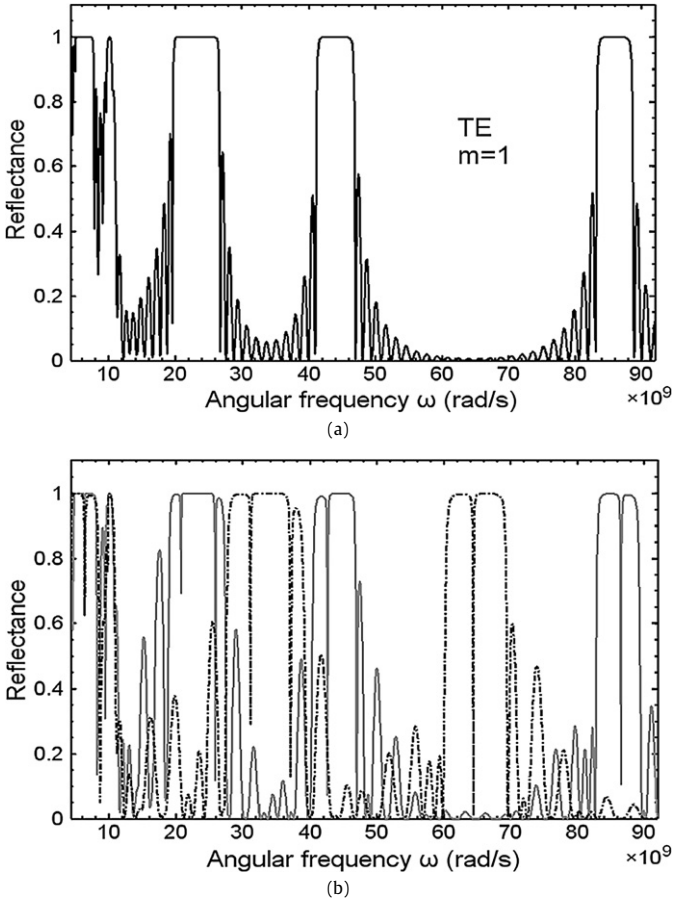

Fig. 10. Calculated reflectance spectra of TE wave at $m = 1$ for the ABR. The material parameters are $a = 1.5$, $b = 1.5$, $\omega_{mp} = 10^{10}$ rad/s, and $\omega_{ep} = 10^{10}$ rad/s. The spectrum with no defect is in (a), where $d_1 = 24$ mm, $d_2 = 12$ mm, $\rho_0 = 30$ mm and $N = 13$. The spectrum of structure with defect layer, is shown in (b), where the defect layer has $\varepsilon_d = 1.8$, $\mu_d = 1.8$ and $d_d = 45$ mm. The gray solid curve is for $d_1 = 24$ mm, $d_2 = 12$ mm. The dash-dotted curve is for $d_1 = 16$ mm, $d_2 = 8$ mm (scaled by 2/3). The starting radius $\rho_0 = 30$ mm is used.

without defect is first plotted in Fig. 10(a). The reflectance in the presence of the defect is then shown in Fig. 10(b), in which two different magnitudes of thickness, $d_1 = 24$ mm, $d_2 = 12$ mm (gray solid curve), and $d_1 = 16$ mm, $d_2 = 8$ mm (dash-dotted curve) are taken, and the starting radius $\rho_0 = 30$ mm is used as well. When the lattice constant is scaled down by 2/3, the Bragg gap in the presence of the defect is obviously moved to the higher frequency, while it remains fixed for the SNG gap. The result again elucidates that the SNG gap is indeed robust to the lattice constant (with a fixed thickness ratio of the constituent bilayer) even in the ABR. It is also contrasted with the Bragg gap that the spectral position of the defect mode inside the SNG gap is nearly invariant with the lattice constant scaling.

4. Summary

The photonic band structures of an ABR containing SNG materials have been theoretically examined in this work. With the field solutions of the circular Bragg waves being dependent on the azimuthal mode number m, optical properties including the SNG and Bragg gaps at different m modes are examined numerically. The conclusion can be drawn as follows. First, at the lowest mode, $m = 0$, the PBG structure in an ABR is nearly identical to that of a PBR. Second, At higher order azimuthal mode $m \geqslant 1$, we find that there is an additional PBG called the MNG gap and the ENG gap for the TE wave and TM wave, respectively. We also find that there exist some reflection dips when ω_{mp} and ω_{ep} are taken in the PBG for TE and TM waves, respectively. These results are closely related to the higher order azimuthal mode of the cylindrical wave in an ABR, which are has not be seen in the PBR with SNG materials. Such special filtering responds make it possible to design the structure of a narrowband resonator without introducing any defect layer to break the periodicity. Third, the PBGs are strongly affected by the starting radius in addition to the m-number at $m > 0$. The SNG gap is robust to the lattice constant with a fixed thickness ratio of the constituent bilayer. Finally, for an ABR including a defect layer, it is found that the property of the SNG band gap is insensitive to the disorder.

Acknowledgement

The authors acknowledge the financial support from the National Science Council of the Republic of China (Taiwan) under grant Nos. NSC-97-2112-M-003-013-MY3 (C.-J. Wu), and NSC-97-2112-M-216-001 (T.-J. Yang), respectively.

References

[1] V.G. Veselago, Sov. Phys. Usp. 10 (1968) 509.
[2] D.R. Smith, W.J. Padilla, D.C. Vier, S.C. Nemat-Nasser, S. Schultz, Phys. Rev. Lett. 84 (2000) 4184.
[3] R.A. Shelby, D.R. Smith, S. Schultz, Science 292 (2001) 77.
[4] J.B. Pendry, Phys. Rev. Lett. 85 (2000) 3966.
[5] H. Jiang, H. Chen, H. Li, Y. Zhang, Appl. Phys. Lett. 83 (2003) 5386.
[6] J. Li, L. Zhou, C.T. Chan, P. Sheng, Phys. Rev. Lett. 90 (2003) 083901.
[7] I.V. Shadrivov, A.A. Sukhorukov, Y.S. Kivshar, Appl. Phys. Lett. 82 (2003) 3820.
[8] J.B. Pendry, A.J. Holden, D.J. Robbins, W.J. Stewart, J. Phys.: Condens. Matter 10 (1998) 4785.
[9] J.B. Pendry, A.J. Holden, D.J. Robbins, W.J. Stewart, IEEE Trans. Microwave Theory Tech. 47 (1999) 2075.
[10] A. Alù, N. Engheta, IEEE Trans. Antennas Propagat. 51 (2003) 2558.
[11] D.R. Fredkin, A. Ron, Appl. Phys. Lett. 81 (2002) 1753.
[12] L.-G. Wang, H. Chen, S.-Y. Zhu, Phys. Rev. B 70 (2004) 245102.
[13] H. Jiang, H. Chen, H. Li, Y. Zhang, J. Zi, S. Zhu, Phys. Rev. E 69 (2004) 066607.
[14] P. Li, Y. Liu, Phys. Lett. A 373 (2009) 1870.
[15] W.M.J. Green, J. Scheuer, G. DeRose, A. Yariv, Appl. Phys. Lett. 85 (2004) 3669.
[16] J. Scheuer, W.M.J. Green, G. DeRose, A. Yariv, Opt. Lett. 29 (2004) 2641.
[17] M.A. Kaliteevski, R.A. Abram, V.V. Nikolaev, G.S. Sokolovski, J. Mod. Opt. 46 (1999) 875.